Effect of Jet Configuration on Knock Characteristics Using a Rapid Compression Machine

Wei Liu [a], Yunliang Qi [a,b], Ridong Zhang [a], Qihang Zhang [a], Zhi Wang [a]

[a] State Key Laboratory of Automotive Safety and Energy, Tsinghua University
Beijing, China

[b] Graduate Aerospace Laboratories, California Institute of Technology
Pasadena, USA

1   Introduction

Jet ignition (JI) is deemed as a promising ignition method in spark ignition (SI) engines since it holds advantages in burning velocity [1], thermal efficiency [2], EGR durability [3], and combustion stability [4] when compared to conventional SI method. However, without changing the nature of premixed combustion, knock occurrence remains possible under JI [5], which is worth studying.

Jet chamber design has vital impacts on jet behaviors including burning velocity and jet configuration, and thus influences knock characteristics. An optimal jet chamber should gain both high burning velocity and low knock intensity at the meantime, whose design should follow specific principles according to the interaction between key parameters regarding knock, e.g., residence time, burned mass fraction at the instant of auto-ignition (BMF_{AI}), knock intensity, and etc.. With the change of burning velocity, various BMF_{AI} and knock intensity might be resulted [6], bringing in contradictions on whether knock intensity increases with increasing BMF_{AI}.

To address the above issues, different jet configurations with different jet hole numbers and angles, were compared under identical initial thermodynamic conditions to investigate the effect of jet configuration on knock characteristics on a rapid compression machine (RCM). The impacts of jet configuration on burning velocity, knock intensity were investigated. The relationship between BMF_{AI} and knock intensity was also discussed.

2   Experimental Setup

2.1 Rapid compression machine

Experiments were conducted on an RCM at Tsinghua University (TU-RCM). Detailed descriptions of TU-RCM can be found in Refs. [7, 8]. A high-accuracy pressure transducer (Kistler 6124A) and a high-speed camera (Photron SA-X2) were used to capture the pressure history and the photography during the combustion process. The pressure signal was sampled at a frequency of 100 kHz. The combustion images were recorded at a resolution of 128×128 pixels with a frame rate of 288000 fps. The spark plug and camera were triggered by the same TTL at the piston's arrival at EOC. The schematic of RCM can be found in Figure 1 (a).
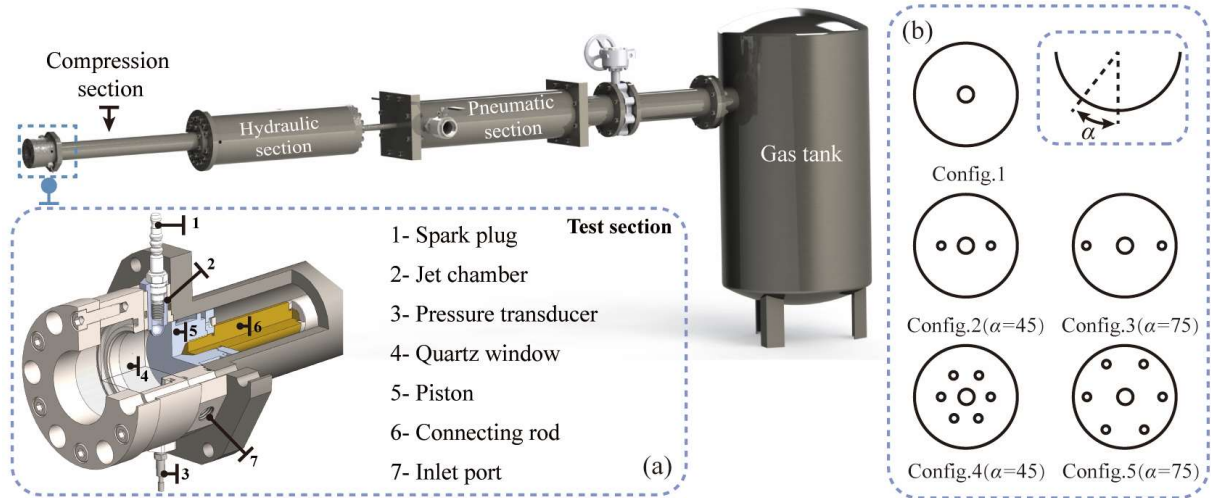
Figure 1 Schematic of the TU-RCM and jet chambers

2.2 Test conditions

Five kinds of jet chambers were tested, whose configurations are shown in Figure 1 (b). The hole numbers were selected as 1/3/7 while the angles between the main hole and side holes were selected as 45° and 75°. The central holes of the five jet chambers have the same size, 3 mm in diameter; so do the peripheral holes, 1.5 mm in diameter.

The mixture composed of *iso*-octane/oxygen/nitrogen/argon was utilized as the test gas, shown in Table 1. Previous work has reported that the knock process of *iso*-octane can be divided into two types depending on whether the auto-ignition process is impacted by low-temperature chemistry (LTC) or not [9]. Inspired by this, the test conditions in this study were selected as (1) Type A (T_{EOC} = 660 K) where LTC has strong impact on end-gas auto-ignition (2) Type B (T_{EOC} = 775 K) where the LTC has little impact, to make this work more comprehensive.

Table 1 Mixture composition and test condition

No.	φ	Mixture composition				Target condition	
		iC_8H_{18}	O_2	N_2	Ar	p_{EOC} [bar]	T_{EOC} [K]
Type A	1	1	12.5	47	0	10-20	660
Type B				13.43	33.57	6-20	775

The thermodynamic trajectories of the end-gas of Type A and Type B under Config.1 were first calculated using Chemkin-Pro [6, 10] and the detailed mechanism from Lawrence Livermore National Laboratory (LLNL) [11, 12], shown in Figure 2. Under Type A, the end-gas auto-ignition evolution started at T_{EOC} = 660 K, traveling across the whole NTC region and finally terminating beyond the upper boundary of the NTC region regardless of initial pressure. The end-gas under Type A was thus thought to be greatly impacted by LTC. For Type B, the evolution trajectory of the end-gas started near the upper boundary of the NTC region while its majority was located in the high-temperature region where LTC has little ascendancy. A similar trend of end-gas evolution can also be found under other configurations (Not exhibited here for brevity).

Figure 3 (a) and (b) demonstrate the pressure traces under Type A and Type B, respectively. According to Ref. [9], for type A, the knock is composed of two or more auto-ignition events while for Type B the auto-ignition only occurs once. For Type A, distinct turning points can be seen on pressure traces before final oscillation, indicating the occurrence of wild-spread auto-ignition which was absent from the cases under Type B. Similar observations were also reported under other configurations.
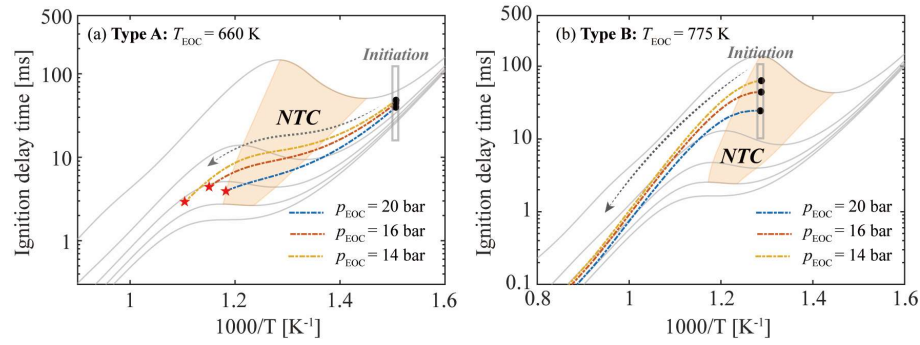
Figure 2 The thermodynamic trajectory of end-gas of Type A and Type B under Config.1 (Gray line group stands for calculated ignition delay time under 10/30/50/70/90 bar. Yellow region stands for NTC region).
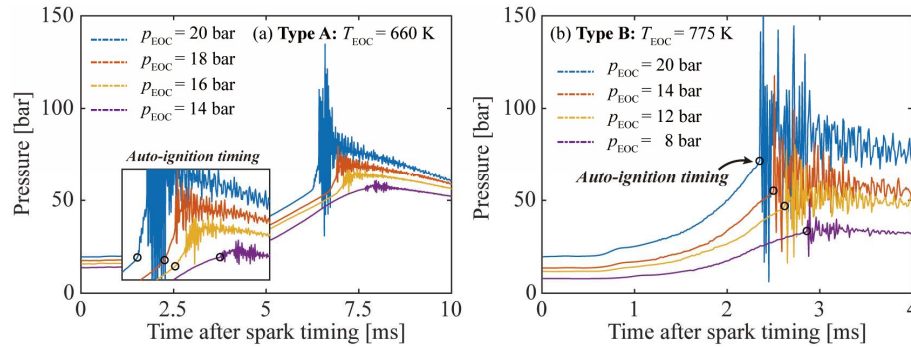
Figure 3 Pressure traces under Type A and B under Config.1 (Circles denote first auto-ignition occurrence)

3   Results

3.1 Knock characteristics

Residence time was selected as the indicator of burning velocity, the variation of residence time is shown in Figure 4 (a). Generally, the residence time decreased with increasing initial thermodynamic conditions. For the cases under Type A, the difference in residence time between each test condition was obvious. As for the cases under Type B, the residence time has been too short to show the difference between each configuration. The jet chambers with multiple holes show faster combustion when compared with the baseline (Config.1), manifested by smaller residence time. However, the fastest burning velocity was derived when using the jet chambers with triple-holes (Config. 2/3) rather than septimal-holes (Config. 4/5). This is due to the competition between two aspects: On one hand, more holes indeed resulted in more beams of jet, which helped increase burning velocity; on the other hand, the mass flow rate will also be increased with the increase in hole number, so the pressure difference between the jet chamber and the main chamber was hard to keep high, which in turn slowed down the jet velocity of each beam. The highest burning velocity should be gained with a moderate hole number.

Figure 4 (b) compares the knock intensity (defined as the integrated high-pass filtered pressure oscillation, shown in Figure 4 (b)) with changing initial pressure and jet configuration. Compared with Config.1, the knock intensity under the configurations with triple-holes (Config.2/3) was smaller while that under configurations with septimal-holes (Config.4/5) didn't show a certain trend. No obvious trend between burning velocity and knock intensity was found. Figure 5 shows the jet flame development processes under each configuration, with T_{EOC} = 660 K and p_{EOC} = 22 bar. By the high-speed images, different flame-auto-ignition interaction behaviors are as follows.
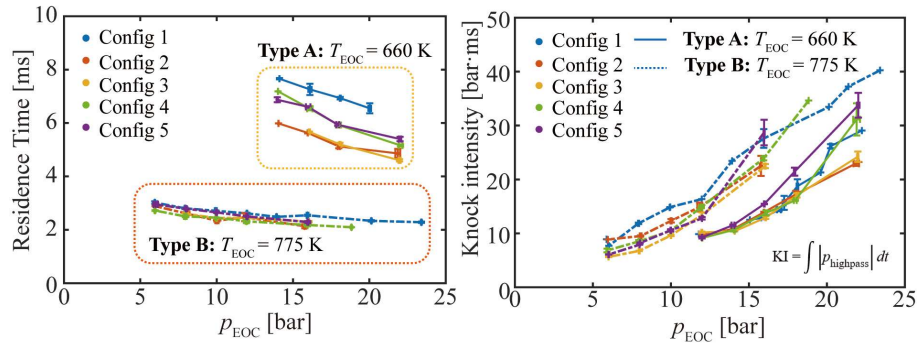
Figure 4 High-speed images of combustion processes under various jet configurations (Numbers on the right-bottom of each image denotes the image enhancement coefficient)

For the single-hole jet chamber, the jet flame propagated straightly towards the opposite chamber wall. After impinging on the wall, the flame continued to propagate laterally. Consequently, the end-gas region was located near the bilateral upper chamber wall. As for the cases with triple-holes (Config.2/3), the three beams of jets propagating in different directions surrounded each other, leaving the end-gas region surrounded by the burned gas. The shock wave generated by end-gas auto-ignition was then decayed or attenuated by the burned region due to the lack of energy sustainment, making its impact on the chamber wall less than baseline. As for the cases with septimal-holes (Config.4/5), the divided jets failed to surround each other, leaving the end-gas region remained near the bilateral bottom of the chamber wall, similar to that under the baseline configuration.
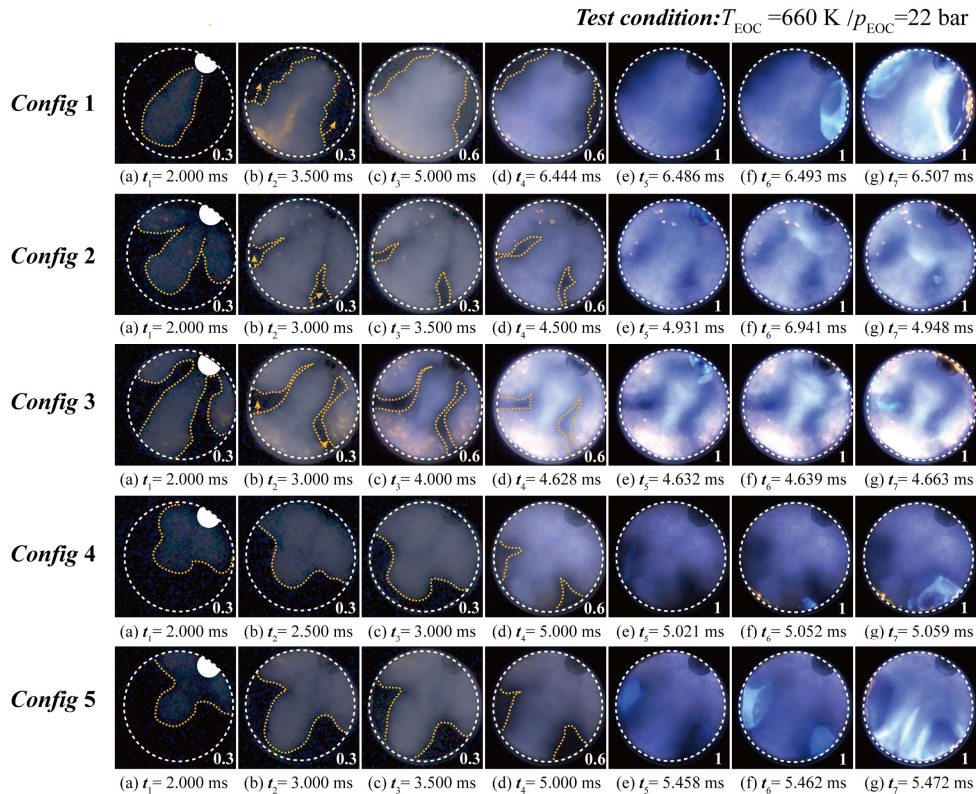
Figure 5 High-speed images of combustion processes under various jet configurations (Numbers on the right-bottom of each image denotes the image enhancement coefficient)

3.2 Auto-ignition regime

According to previous studies, the effect of burned mass fraction at the instant of auto-ignition (BMF$_{AI}$) on knock tendency remained unclear, especially under jet ignition. An increasing knock intensity was

found with the increasing BMF_{AI} [13-15] while opposite result was reported in Ref.[16]. The contradictions on the BMF_{AI} were then interpreted by Yu et al. that a transition from isochoric to isobaric combustion of the end-gas led to a compromise of the maximum pressure [17]. Nevertheless, the relationship between the BMF_{AI} and the knock tendency demands more investigation. In the present work, the BMF_{AI} was calculated based on Eq. 1 where p_{eq} represents the calculated chemical equilibrium pressure based on mixture initial condition while p_{ai} stands for the pressure at the instant of auto-ignition event.

$$BMF_{AI} = \frac{p_{ai} - p_{EOC}}{p_{eq} - p_{EOC}} \qquad\qquad \text{Eq. 1}$$

The relationship between knock intensity and BMF_{AI} is depicted in Figure 6 (a). The knock intensity was suppressed with the increasing BMF_{AI} for both Type A and Type B. The auto-ignition mode also tended to degrade from detonation to non-detonation with the increasing BMF_{AI}. Noticing that, the knock intensity was more sensitive to the variation in BMF_{AI} under Type B than Type A did. This might be ascribed to the fact that there was only one auto-ignition event under Type B, so the knock intensity was directly affected by the intensity of the only auto-ignition. The less the BMF_{AI}, the more residual energy the end-gas can provide to support the shock wave. Thus, the BMF_{AI} had a direct impact on the final knock intensity. For the cases under Type A, however, the auto-ignition initiation process was more complicated as there were multiple auto-ignition events during the whole knock process. These auto-ignition events interacted with each other, leading to the final pressure oscillation. So the intensity of the final pressure oscillation depended not only on the first auto-ignition event but also on the extent to which the thermos-acoustic coupling may achieve during the period from first auto-ignition to the final oscillation [9].
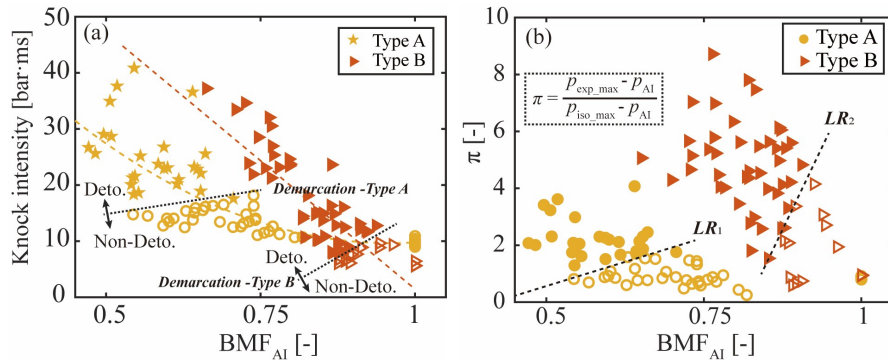
Figure 6 Relationship between knock intensity and burned mass fraction.

Another dimensionless parameter, π was then calculated to take the influence of the knock intensity into account [18]. The π was calculated based on: p_{AI} the pressure at the moment of auto-ignition, p_{exp_max} the maximum experimental pressure, p_{iso_max} the maximum pressure obtained from theoretical isochoric combustion. The relationship between the BMF_{AI} and π is depicted in Figure 6 (b), the definition of π is also shown.

Generally, the larger the BMF_{AI}, the lower the π, which was consistent with the results in Figure 6 (a) since stronger knock was likely to occur with larger π. Detonation tended to occur with low BMF_{AI} and high π for both Type A and Type B. Distinct boundaries can be obtained using logistic regression method to distinguish detonation. It is clear that detonation onset tended to occur with less unburned mixture under Type B than Type A. No detonation was found when the BMF_{AI} exceeded 0.75 under Type A while a BMF_{AI} of 0.8 was still sufficient to initiate the detonation under Type B.

Conclusions

Knock characteristics and auto-ignition behaviors of end-gas under various jet configurations were investigated using an RCM. With the increase of jet holes, the residence time was first shortened and then prolonged. The fastest burning velocity was achieved with triple-hole jet chamber, which is due to

the competition between the pressure build up and the mass loss rate in the jet chamber with jet hole number increases. The effect of jet angles lied in the location of the end-gas region, which plays a vital role in determining knock intensity. The jet configurations which can make the end-gas surrounded by the jet flames is favorable to knock mitigation. In the current work, the jet chamber configurations with triple-holes hold strong points in both burning velocity enhancement and knock suppression. The BMF_{AI} - π diagram was then applied to identify auto-ignition modes. The knock intensity was more sensitive to the variation of BMF_{AI} under Type B than Type A did. It was suggested that detonation tended to occur with low BMF_{AI} and high π for both Type A and Type B conditions. Detonation and non-detonation cases could be clearly demarcated in the BMF_{AI} - π diagram. The detonation cases called for less unburned mixture under Type B than Type A.

References

[1] Elisa, Toulson, Andrew, Huisjen, Xuefei, Chen, Cody, Squibb, Guoming, Z.J.S.I.J.o. Engines, Visualization of Propane and Natural Gas Spark Ignition and Turbulent Jet Ignition Combustion, (2012).

[2] Z. Zhao, Z. Wang, Y. Qi, K. Cai, F.J.I.J.o.E.R. Li, Experimental study of combustion strategy for jet ignition on a natural gas engine, (2020) 146808742097775.

[3] S. Tolou, H.J.I.J.o.E.R. Schock, Experiments and modeling of a dual-mode, turbulent jet ignition engine, 21 (2019) 146808741987588.

[4] J. Hua, L. Zhou, Q. Gao, Z. Feng, H. Wei, Effects on Cycle-to-Cycle Variations and Knocking Combustion of Turbulent Jet Ignition (TJI) with a Small Volume Pre-Chamber, SAE International, 2020.

[5] P. Litke, W.P. Attard, H. Blaxill, E.K. Anderson, Knock Limit Extension with a Gasoline Fueled Pre-Chamber Jet Igniter in a Modern Vehicle Powertrain, SAE International Journal of Engines 5 (2012) 1201-1215.

[6] W. Liu, Y. Qi, X. He, Z. Wang, Investigation on Effects of Ignition Configurations on Knocking Combustion Using an Optical Rapid Compression Machine under Lean to Stoichiometric Conditions, J Combustion Science Technology, (2020) 1-22.

[7] H.S. Di, X. He, P. Zhang, Z. Wang, M.S. Wooldridge, C.K. Law, C.P. Wang, S.J. Shuai, J.X. Wang, Effects of buffer gas composition on low temperature ignition of iso-octane and n-heptane, Combustion and Flame 161 (2014) 2531-2538.

[8] W. Ji, P. Zhang, T. He, Z. Wang, L. Tao, X. He, C.K. Law, Intermediate species measurement during iso-butanol auto-ignition, Combustion and Flame 162 (2015) 3541-3553.

[9] W. Liu, Y. Qi, R. Zhang, Z. Wang, Flame propagation and auto-ignition behavior of iso-octane across the negative temperature coefficient (NTC) region on a rapid compression machine, Combustion and Flame, doi:https://doi.org/10.1016/j.combustflame.2021.111688(2021) 111688.

[10] Y. Qi, Y. Wang, Y. Li, J. Wang, X. He, Z. Wang, Auto-ignition characteristics of end-gas in a rapid compression machine under super-knock conditions, Combustion and Flame 205 (2019) 378-388.

[11] H.J. Curran, P. Gaffuri, W.J. Pitz, C.K. Westbrook, A comprehensive modeling study of n-heptane oxidation, Combustion and flame 114 (1998) 149-177.

[12] H.J. Curran, P. Gaffuri, W.J. Pitz, C.K. Westbrook, A comprehensive modeling study of iso-octane oxidation, Combustion and flame 129 (2002) 253-280.

[13] G.A. Karim, A dimensionless criterion for predicting the onset of knock in spark ignition engines, Report No. 0148-7191, SAE Technical Paper, 2004.

[14] L. Kagan, G. Sivashinsky, Hydrodynamic aspects of end-gas autoignition, Proceedings of the Combustion Institute 34 (2013) 857-863.

[15] L.S. Kagan, P.V. Gordon, G.I. Sivashinsky, A minimal model for end-gas autoignition, Combustion Theory and ModellingCombustion Theory and Modelling 16 (2012) 1-12.

[16] A. Robert, S. Richard, O. Colin, T. Poinsot, LES study of deflagration to detonation mechanisms in a downsized spark ignition engine, Combustion and Flame 162 (2015) 2788-2807.

[17] H. Yu, C. Qi, Z.J.P.o.t.C.I. Chen, Effects of flame propagation speed and chamber size on end-gas autoignition, 36 (2017) 3533-3541.

[18] J. Rudloff, J.-M. Zaccardi, S. Richard, J. Anderlohr, Analysis of pre-ignition in highly charged SI engines: Emphasis on the auto-ignition mode, Proceedings of the Combustion Institute 34 (2013) 2959-2967.